



Eidgenössische Technische Hochschule Zürich
Swiss Federal Institute of Technology Zurich

Dielectric Loss Study in Superconducting Coplanar Waveguide Resonators

Semester Paper 2014 Fall

Junxin Chen

March 18, 2015

Advisors: M. Oppliger, Prof. Dr. A. Wallraff

Department of Physics, ETH Zürich

Abstract

Decoherence is one of the major limitations of superconducting circuit as an architecture of quantum information processing and scalable quantum computation. Below the critical temperature of the superconductor, dielectric loss is one of the most significant channels of decoherence. This semester paper explores the possibility to reduce dielectric loss and the geometry dependence of quality factors of the coplanar waveguide resonators by changing the design of the resonator in various simulators. Reducing contamination on interfaces by surface treatment and etching into substrate below CPW gap are found helpful in reducing dielectric loss in CPW resonators.

Contents

Contents	iii
1 Introduction	1
1.1 Coplanar Waveguide Resonator	2
1.1.1 Fabrication	3
1.1.2 Basic Resonator Properties	4
1.2 Decoherence	5
1.3 Quality Factor	5
2 Dielectric Loss Study	9
2.1 THz Resonators	10
2.1.1 Parametric Sweep in Metal-Substrate Contamination Model	11
2.1.2 Etch Depth Sweep in Substrate-Air Contamination Model	14
2.1.3 Contamination Comparison	15
2.2 GHz Resonators	17
2.2.1 Parametric Sweep	18
2.2.2 Etch Depth Study	18
2.2.3 Contamination Comparison	21
2.3 Discussion	21
2.3.1 Modeling with COMSOL	22
2.3.2 Etch Depth and Dielectric Loss	23
2.4 Conclusion and Outlook	24
A COMSOL RF Module Manual	25
A.1 Build A New Model	25
A.2 Global Parameters	25
A.3 Port and Lumped Port	26
A.4 Mesh	27
A.5 Eigenfrequency Study	27

CONTENTS

A.5.1 Graphics Window	28
B SONNET Manual	31
C Xmon Capacitor	35
Bibliography	37

Chapter 1

Introduction

Quantum mechanics provides the possibility of computing some problems much faster than classical computers^[1, 2], and the possibility of theoretically secure communication^[3]. To achieve the protocols, quantum bit (qubit), the quantum counterpart of classical bit, should be developed. A reasonable qubit for scalable quantum computing should satisfy several criteria named after D. DiVincenzo^[4]:

1. identification of well-defined qubits;
2. reliable state preparation;
3. low decoherence;
4. accurate quantum gate operation;
5. accurate quantum measurement;

and two extra criteria^[5]:

1. information in stationary qubit can be converted to flying qubit with high fidelity and
2. reliable transfer of flying qubit.

Superconducting circuit based qubits satisfy most of the criteria well. The possibility of non-demolition measurement of the qubit state^[6, 7], the potential in scalability^[8], and the relative high fidelity of single-qubit and multi-qubit gate operations^[9, 10] make superconducting circuit based qubit one of the most promising candidates of qubit. However, relatively short coherence time limits the overall performance of superconducting circuit. This thesis focuses on dielectric loss, one of the origins of decoherence.

1.1 Coplanar Waveguide Resonator

A coplanar waveguide resonator (CPW resonator) is an on-chip microwave analogy for optical cavity. In superconducting circuit, coplanar waveguide resonator is a key element in on-chip quantum information processing like photon detection^[11], quantum computation^[8, 10], narrow-band filters^[12] etcetera. A typical structure of a CPW resonator is shown in Figure 1.1. Purple colored parts are superconductor elements: input/output port, central line, ground plane grown on substrate. Gaps between superconductor elements are coupling capacitor and waveguide gap. When connected to a circuit, a CPW resonator is equivalent to an LC resonator, as the coupling capacitors provide some portion of capacitance and central line provides inductance and the rest capacitance.

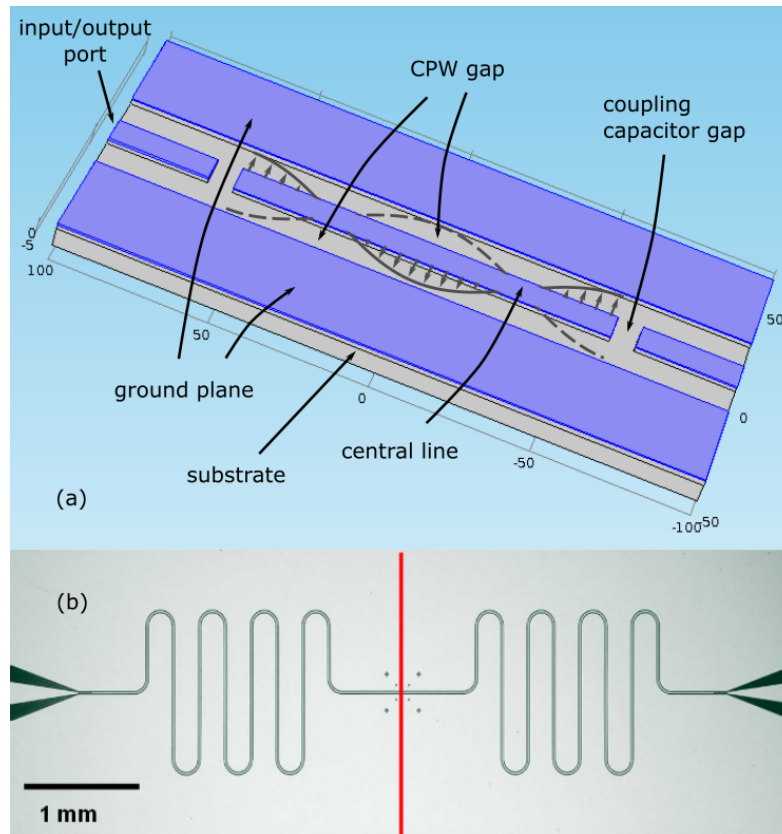


Figure 1.1: (a) Structure of CPW resonator, where purple parts are superconductors and gray part is substrate; (b) an optical microscope image of CPW resonator^[13]

In a coplanar waveguide shown in Figure 1.1, more than one modes are supported^[14], among which odd and even modes are two primary ones. Odd mode distributes between two ground planes, and is usually consid-

ered as parasitic. This mode can be avoided by connecting two ground planes. As for even mode, electromagnetic wave propagates in the CPW gap, and is mostly confined in the plane of conductor. Even mode is the mode utilized in most cases, so is in this semester paper. When capacitor gaps are introduced, standing waves with wavelength $\lambda = \frac{2L}{n}$ (L is the length of central line, n is a positive integer) appear between two capacitor gaps. As an analogy for LC resonator, at coupling capacitor gaps are anti-nodes of electromagnetic field.

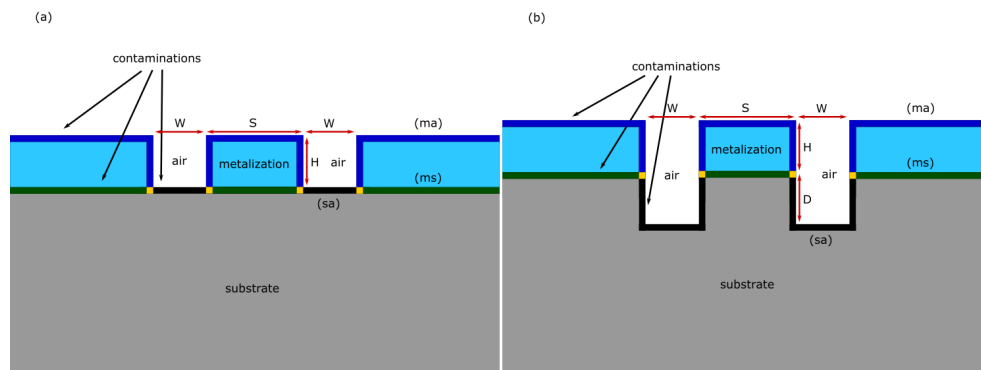


Figure 1.2: Typical cross-sectional sketches of CPW resonators. The contaminations at interfaces are the main source of dielectric loss. (a) A design without etching into substrate, where W is CPW gap width, S is central line width, and H is metal thickness; (b) a design with etching into substrate at CPW and capacitor gaps, where the extra parameter D is the etch depth.

Figure 1.2 shows two typical cross-sectional designs of CPW, with one etching into substrate and the other not. The differences between the two designs will be compared in Chapter 2.

1.1.1 Fabrication

Superconducting CPW resonators can be fabricated by photolithography treatment on substrate followed by evaporating metal layer on it^[13]. Basic procedure of photolithography is as follows^[15]:

1. clean the substrate to remove organic or inorganic contaminations;
2. coat viscous liquid solution of photoresist by spin coating, which results in a uniform thin layer;
3. align prefabricated photo mask on the wafer, and expose it in UV light to remove photoresist at designed position (gaps in CPW resonator case);
4. etch into the substrate by liquid or plasma chemical agent;
5. remove photoresist.

After photolithography, the substrate is metalized with materials like Al by electron beam evaporation, and lifted-off with hot acetone. This step finalizes the fabrication of a CPW resonator.

1.1.2 Basic Resonator Properties

Fundamental frequency f_0 and characteristic impedance are two most basic properties of a CPW resonator^[13], where f_0 is given by

$$f_0 = \frac{c}{\sqrt{\epsilon_{eff}}} \frac{1}{2l} \quad (1.1)$$

where c is speed of light in vacuum, l is the resonator length, and ϵ_{eff} is effective permittivity, which depends on the material of CPW resonator and its geometry. Equation 1.1 allows determining ϵ_{eff} , when the fundamental frequency of the CPW resonator is available. By definition, phase velocity in the CPW is given by $v_{ph} = c/\sqrt{\epsilon_{eff}} = 1/\sqrt{L_l C_l}$, where L_l and C_l are the capacitance and inductance per unit length of the coplanar waveguide. By conformal mapping techniques, L_l and C_l are given by^[16, 17]

$$L_l = \frac{\mu_0 K(k'_0)}{4 K(k_0)} \quad (1.2)$$

$$C_l = 4\epsilon_0\epsilon_{eff} \frac{K(k_0)}{K(k'_0)} \quad (1.3)$$

where K is the complete elliptic integral of the first kind with geometric arguments

$$k_0 = \frac{S}{S + 2W_g} \quad (1.4)$$

$$k'_0 = \sqrt{1 - k_0^2} \quad (1.5)$$

where S is central line width, and W_g is the CPW gap width (gap between central line and ground plane).

Then the characteristic impedance of a CPW is given by

$$Z_0 = \sqrt{L_l/C_l} = \frac{1}{4} \sqrt{\frac{\mu_0}{\epsilon_0\epsilon_{eff}}} \frac{K(k'_0)}{K(k_0)} \quad (1.6)$$

1.2 Decoherence

Decoherence is the process of quantum system losing coherence when couple to the environment. Decoherence can be classified into thermal excitation, relaxation and dephasing. Thermal excitation is the process of incoherently exciting the quantum system through thermal fluctuation, which can be suppressed effectively by cooling the system. Relaxation is the process of a qubit relaxing from excited state to ground state, which randomizes the phase of the system; in quantum information context, characteristic relaxation time is usually referred as T_1 . In superconducting circuit, relaxation may be caused by spontaneous emission, Purcell effect, dielectric loss, quasiparticle tunneling, flux coupling *etc.*^[18]. Dephasing is the process of a qubit losing phase information; characteristic dephasing time is usually referred as T_2 . In superconducting circuit, dephasing may be caused by charge noise, flux noise, critical current noise, E_C noise and quasiparticle tunneling^[18].

Among all the decoherence channels, dielectric loss is a significant one. The origin of dielectric loss has been found to related to two-level states (TLSs) in contaminations distributed mainly on the various interfaces of a coplanar waveguide and related to disorder close to the surface of a crystal^[19, 20, 21], as indicated in figure 1.2. Typically, dielectric loss in contamination is much larger than that in disordered crystal close to surface. Sapphire is a commonly used material of substrate, due to its low dielectric loss. A recent work indicates that Hydrogen bonds in Al_2O_3 play a role in dielectric loss, by tunneling Hydrogen atom between two neighboring Oxygen atoms^[22, 21]. The loss mechanism of tunneling is introduced in reference [22]. To enable tunneling, the potential has to be in coincidence configuration (see figure 1.3 for detail), which usually happens on the interfaces, where the distance among atoms deviates from that in the bulk crystal. The authors of reference [21] also pointed out that this loss mechanism is ubiquitous, because Hydrogen is a common impurity in metal oxides. A direct hint from this work is to reduce exposure to water vapor and acid, and to use plasma (dry) etch method instead of liquid agent when fabricating CPW resonators. In our lab, plasma etching method is used. However, more work could be done to investigate the differences between the two etching methods.

Although the mechanism of dielectric loss is still not well understood, some intuitive ways of reducing its effect mainly by modifying the geometry of CPW are introduced^[20, 23]. The effect of those methods will be discussed in Chapter 2.

1.3 Quality Factor

The quality factor (Q factor) is a dimensionless parameter indicating rate of energy loss relative to the stored energy of a resonator^[24]. Electromagnetism

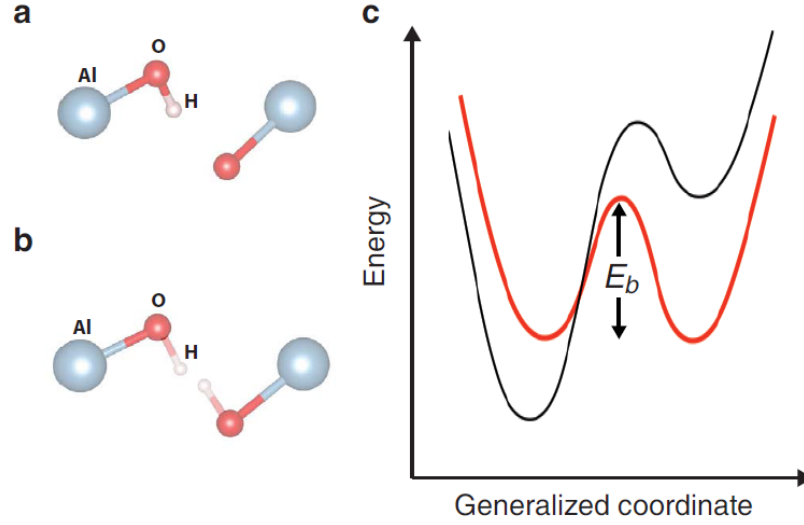


Figure 1.3: ^[21] Self-trapped and coincidence configurations. (a) Geometry of the self-trapped configuration for a hydrogen interstitial in Al₂O₃. H is bonded primarily to a specific O atom, but could alternatively be bonded to a next nearest neighbor O atom. Al atoms are represented by large (grey) spheres, O atoms by smaller (red) spheres, and H atoms by the smallest (pink) spheres. (b) Geometry of a coincidence configuration, obtained by averaging over two adjacent self-trapped configurations. The two symmetric hydrogen sites are indicated by semi-transparent bonds. (c) Schematic potential-energy curve for the self-trapped (black) versus the coincidence (red) configurations. The latter corresponds to a double-well system with energy barrier E_b.

states that electric field can be written as $\vec{E}(\vec{r}, t) = \vec{E}(\vec{r})e^{(-\zeta+i\omega)t}$ for the most of the time, where ζ controls growing and decaying of electric field amplitude over time, and ω is the angular frequency. Subsequently, the definition of Q factor is

$$Q = \frac{\omega}{2\zeta} \quad (1.1)$$

In general, the definition here is not the intrinsic Q factor of a resonator but the so called loaded Q factor (Q_L), if the resonator is loaded to an external circuit^[13]. One can recover intrinsic Q factor using

$$Q_0 = (1 + g)Q_L = \left(1 + \frac{S_{21}(\omega_n)}{1 - S_{21}(\omega_n)}\right)Q_L = \frac{Q_L}{1 - S_{21}(\omega_n)} \quad (1.2)$$

in the context of two-port measurement, where g is the so called coupling constant, and $S_{21}(\omega_n)$ is the S parameter from port 1 to port 2 at resonance frequency of nth harmonic (0 stands for fundamental) ω_n . Alternatively, one can determine Q_L by looking at the resonance peak of a resonator

$$Q_L = \frac{f_n}{\sigma_{bw}} \quad (1.3)$$

where f_n is the resonance frequency of n th harmonic, and σ_{bw} is the bandwidth of the resonance peak. Subsequently, one can determine the intrinsic Q factor of a resonator in two-port measurement by

$$Q_0 = \frac{f_n}{\sigma_{bw}} \frac{1}{(1 - S_{21}(\omega_n))} \quad (1.4)$$

For a resonator without resistive loss, which is valid in our case of superconducting CPW resonator, the intrinsic Q factor Q_0 is determined by

$$Q_0 = \frac{1}{\tan\delta} \quad (1.5)$$

where $\tan\delta$ is the effective dielectric loss of the resonator (see Chapter 2 for detail). Thus, intrinsic Q factor of a superconducting CPW resonator is related to the effect of dielectric loss in the structure. As direct study of dielectric loss is difficult, coplanar waveguide resonators provide an easy way to approach the effect of dielectric loss by studying its effect on the intrinsic quality factor (Q factor) of a resonator^[20]. High Q factor is also required for various tasks involving CPW resonator, for high Q factor means low decoherence in the circuit. In our lab, for example, high Q resonators can be used as a prob to the quality of fabrication methods and the shielding effect of the sample boxes.

Dielectric Loss Study

Dielectric loss is an intrinsic property of a certain dielectric material, which can be well described by a physical quantity called loss tangent^[25]. Electromagnetism points out that dielectric permittivity of a material can be written in the form of $\epsilon_d(\omega) = \epsilon'_d(\omega) - i\epsilon''_d(\omega)$ in general, where ω is the frequency of electromagnetic field^[25]. Real part of the complex dielectric permittivity is mainly responsible for reaction to electric field. Imaginary part is non-zero when there is finite dielectric loss, as an analogy for resistive loss in metal. Loss tangent is then defined as

$$\tan\delta = \frac{\sigma_c(\omega) + \omega\epsilon''_d(\omega)}{\omega\epsilon'_d(\omega)} \quad (2.1)$$

where σ_c is electric conductivity of the material. In our case, σ_c is zero in general, then loss tangent can be reduced to

$$\tan\delta = \frac{\epsilon''_d(\omega)}{\epsilon'_d(\omega)} \quad (2.2)$$

There is evidence showing that, in a CPW resonator, dielectric loss is proportional to the electric field experienced by the lossy materials like contaminations^[20]; the stronger the electric field is, and the more lossy material "sees" electric field, the larger the dielectric loss is. So the direct way of reducing dielectric loss is to reduce contaminations on the surface of the CPW resonator by surface treatment. However, the technology by far cannot totally remove the lossy materials, and results in some unsatisfactory Q factor^[20], which calls for other parallel methods to improve the performance. An indirect way of reducing the effect of dielectric loss in a CPW resonator is to modify its geometry to reduce the electric field amplitude at interfaces, and to reduce lossy material available for electric field.

As mentioned in Section 1.3, dielectric loss study is conducted in coplanar waveguide resonator. Only simulation work is done in this semester paper. Simulation softwares used are COMSOL, SONNET and Microwave Office, for which some basic manual can be found in appendices. None of the software can fully satisfy the requirements of this study, combining their results gives a more comprehensive picture.

2.1 THz Resonators

In this section, COMSOL is the primary simulator. Due to the limitation of COMSOL and limitation in calculation power, resonators of resonance frequency in THz regime instead of GHz regime are simulated. The detailed discussion can be found in subsection 2.1.1.

COMSOL Multiphysics is a powerful simulation tool designed for various physical problems, including electromagnetism, circuit analysis, mechanics, fluid dynamics, heat diffusion etcetera. In this paper RF module is used, which is designed for radio frequency analysis.

In COMSOL, one can draw a model directly, and adjust the geometry of the model conveniently by using self-defined parameters. Parameter sweeping function enables automatic run-time adjustment of model geometry. Importing geometry from a file built by other software like AutoCAD is also allowed. This function makes it possible to analyze models with complicated geometry consisting of non-standard shapes. However, sweeping geometric parameters is forbidden in this function. Livelink between COMSOL and geometry design software can resolve the problem.

In our models, angle δ in loss tangent of contaminations are uniformly set to be 0.002, which is a reasonable value of contaminations on the interfaces of superconducting CPW^[20]. The material of substrate is sapphire, a common substrate material, whose relative dielectric constant is anisotropic:

$$\begin{pmatrix} 9.3 & 0 & 0 \\ 0 & 9.3 & 0 \\ 0 & 0 & 11.5 \end{pmatrix} \quad (2.1)$$

Contaminations are modeled by thin layers of sapphire with certain loss tangent. Though, in principle, it is possible to model it with transition boundary condition (an easier way), we did not manage to achieve that, as it is hard to find the manual teaching the usage of a certain function in COMSOL. To simulate the effect of superconductor, all conductors in the model are perfect conductors. (There is no built-in perfect conductor in COMSOL. Self-built material with purely imaginary permittivity with large imaginary

part ($-10^{15}i$) is used instead, where minus sign is the convention used by COMSOL.)

Figure 1.1 (a) is a screen shot of a CPW resonator model in COMSOL without substrate and with above air blocks hidden.

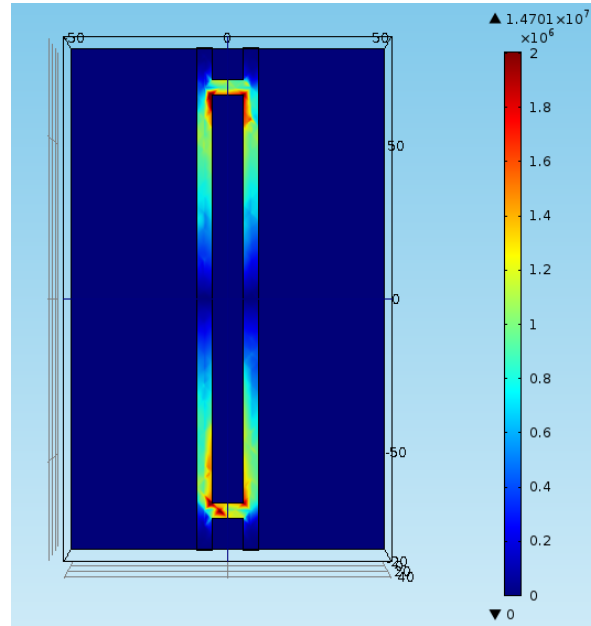


Figure 2.1: COMSOL simulation of electric field norm distribution in a CPW resonator

Eigenfrequency study around fundamental frequency of the resonator gives a electric field norm distribution shown in Figure 2.1. The simulation is consistent with the theoretical description in Chapter 1, in the sense of finding anti-node at coupling capacitor gaps, while node at center of the resonator for fundamental frequency. The slightly asymmetric distribution is a result of the asymmetric automatic mesh.

Eigenfrequency study also enables determining Q factor of the model, which follows the definition (1.1). Although the measured Q factor is loaded Q, it reflects dielectric loss reliably as long as the intrinsic impedance of the CPW resonator matches port impedance.

2.1.1 Parametric Sweep in Metal-Substrate Contamination Model

The table 2.1 lists different parameters swept in the simulation, the corresponding parameter symbol, and the standard value (the value when the parameter is not swept).

In the simulation, S , W , W_g and d_{cont} are typical values in a CPW resonator^[13, 20]. However, L is 100 times smaller than a typical value in superconducting

Table 2.1: COMSOL parameter list

parameters	symbols	standard value
resonator length	L	130 (um)
central line width	S	10 (um)
coupling capacitor gap width	W	4 (um)
CPW gap width	W_g	4 (um)
contamination thickness	d_{cont}	2 (nm)
etch depth into substrate	d_{etch}	8 (nm)

circuit based quantum information processing, leading to a resonance frequency in THz regime, 100 times larger than the typical one. Limitation of calculation power is responsible for this mismatch; because the consumption of memory increases linearly with the length of resonator, when the mesh resolution remains the same. The current model already consumes all the memory, even though the mesh is reasonably coarse. The big fluctuations in Q factor in the simulation is an evidence of coarse mesh. Though the frequency is 100 times larger than the typical one, one might argue that the simulation of dielectric loss is still plausible; because all properties in the simulation are frequency-independent. We will see later that the simulation in Sonnet in GHz regime confirms the argument. What is more, the etch depth into substrate is also relatively small. Again, limitation of calculation power makes it hard to simulate deep etching model with the same meshing strategy used above (see Appendix A for detail); because deeper etching requires more mesh sweeping layers to resolve the geometry. In the model with deep etch and different meshing strategy, no resonance mode was found, which is problematic.

Figure 2.2 shows different parameter dependence of Q factor of a model with metal-substrate interface contaminations only (some technical problems prevent us from sweeping the parameters in a full contamination model). Port impedance adjustment is required for S and W_g sweeping. (In principle, it is also necessary for d_{etch} sweeping, but the change of circuit impedance is negligible in the range of d_{etch} sweeping. This point will be clarified in Section ??.)

From figure 2.2 contamination thickness sweep shows a clear correlation with Q factor, which is a nearly perfect power law with exponent -0.937. This result is intuitively understandable: thicker contamination implies larger amount of available lossy material for electric field. A more systematic interpretation is given in [20]. The total effective loss tangent is given by $\sum_i = p_i \tan \delta_i$, where the sum is over different interfaces, and the participation ratio p_i is given by^[20, 18, 26]

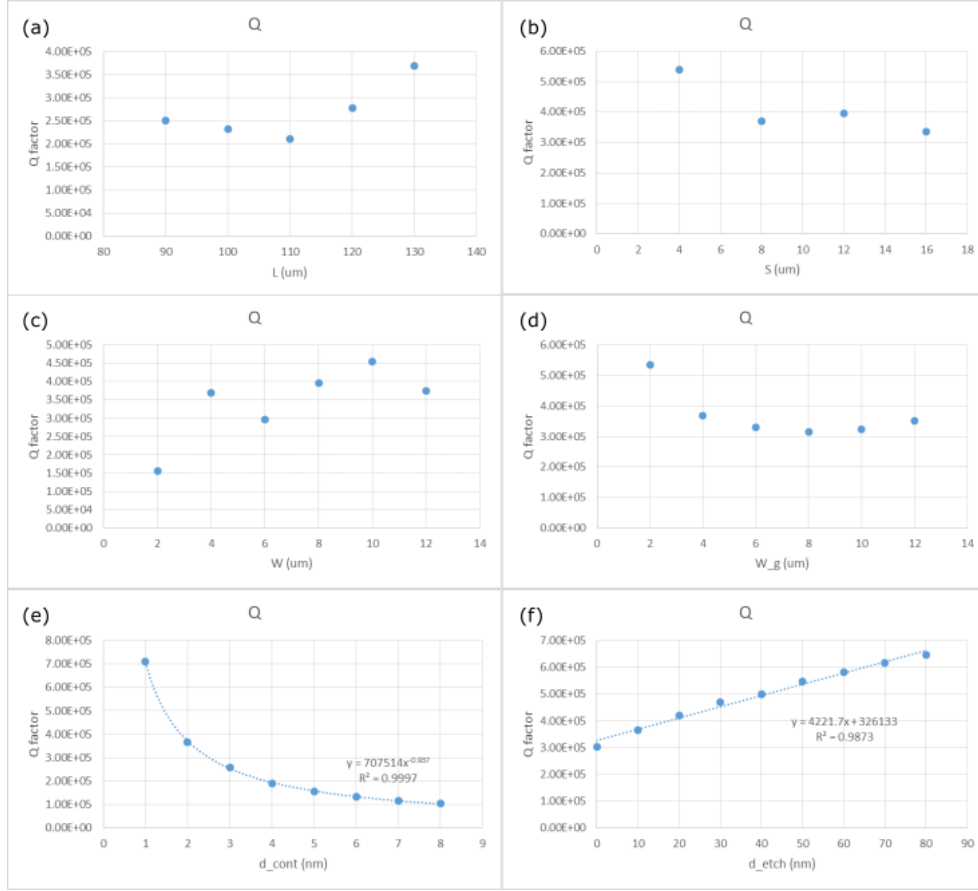


Figure 2.2: Simulated Q factor in COMSOL for a model with ms contaminations only: (a) sweep resonator length; (b) sweep central line width; (c) sweep coupling capacitor gap width; (d) sweep CPW gap width; (e) sweep contamination thickness; (f) sweep etch depth into substrate.

$$p_i = W^{-1}d_i\varepsilon_i \int ds|E|^2 \quad (2.2)$$

where W is energy per unit length, d_i is contamination thickness, and ε_i is dielectric constant. By equation 1.5, in the condition lossless metal, Q factor should be proportional to d_{cont}^{-1} , with some possible deviation due to the difference between loaded Q and intrinsic Q and some fluctuation in the simulation. The result of d_{cont} sweep agrees well with the prediction.

Another noticeable result is a nearly linear increase in the sweep of d_{etch} , which is probably caused by a modeling problem with COMSOL, leaving the dependence unclear. This problem is discussed in subsection 2.1.2.

In general, the fluctuations of Q factor in L , S , W and W_g sweep are much larger than that of d_{cont} and d_{etch} sweep. It is due to different meshing

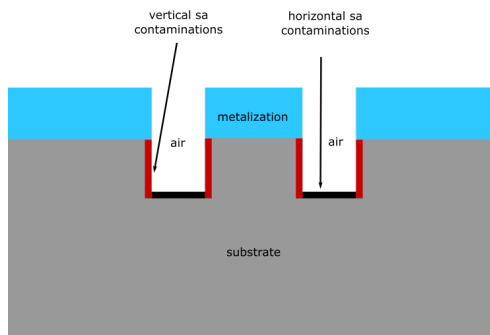


Figure 2.3: The cross section of the models simulated in this subsection. Only substrate-air contaminations are studied.

method. In L , S , W and W_g sweep, COMSOL rebuilds the mesh in the region where geometry is modified, which leaves fluctuation in meshing itself. However, in d_{cont} and d_{etch} sweep, mesh sweeping method (a standard meshing method for thin layer, see Appendix A for detail) keeps the mesh pattern essentially the same during the parametric sweeping. Keeping this in mind, we may conclude that L , S , W and W_g have no significant effect on Q factor in the range we sweeping the parameters.

2.1.2 Etch Depth Sweep in Substrate-Air Contamination Model

Intuitively, etching into substrate changes the effect of dielectric loss on substrate-air interface most. So in addition to the parametric sweep of a model with metal-substrate contamination, d_{etch} dependence of Q factors of models with substrate-air contaminations is simulated. In order to apply mesh sweeping method, the range of d_{etch} sweeping is from 0.1 micron to 0.8 micron, which is comparable to the thickness of conductor.

As the effect of etching on dielectric loss on vertical substrate- air contamination cannot be studied in section 2.1, in addition to the full SA contamination model, a model with only vertical SA contamination is simulated.

The simulation results are shown in figure 2.4. Noticeably, all diagrams shows a linear positive correlation between Q factor and d_{etch} , and the Q factors are of the same order. The result of lossless model indicates that the increasing is not physical, but some modeling problem in COMSOL.

To avoid the modeling problem, we treat the result of lossless model as background and subtract the effect of the background. Recall that in a model without resistive loss, the intrinsic Q factor is just the inversion of effective dielectric loss tangent (equation 1.5), and it is reasonable to do addition or subtraction on effective loss tangent. So we first inverse the Q factors, then

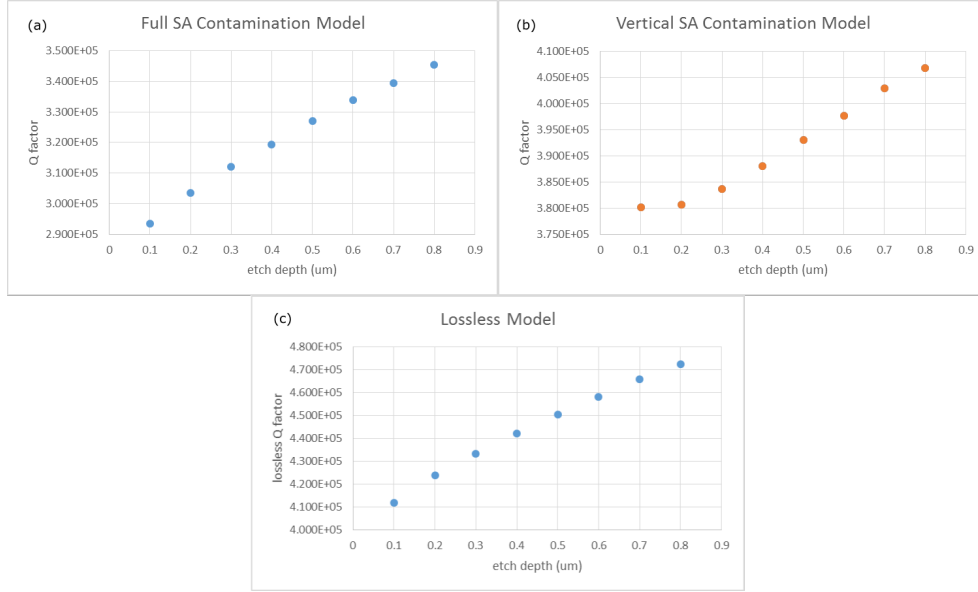


Figure 2.4: Simulated etch depth dependence of Q factor in COMSOL: (a) result of a model with full substrate-air contamination; (b) result of a model with vertical substrate-air contamination only; (c) result of a lossless model.

subtract the effective loss tangent of lossless model from the value of lossy models, and finally conduct inversion again to get back Q factors.

The resulted Q factors are shown in figure 2.5. Q factor of vertical SA contamination follows a shifted power law with respect to d_{etch} with the power exponent around -1. The negative correlation is expected, as etching into substrate increases the area of vertical contamination. Q factor of full SA contamination model shows a pretty linear positive correlation with d_{etch} , which infer that the decreasing of dielectric loss on the horizontal SA interface wins the competition against the increasing on the vertical interface. The effect of etching on dielectric loss on horizontal SA interface is studied in detail in section 2.2. The result of full SA contamination model suggests etching into substrate to obtain a higher Q factor of a CPW resonator.

2.1.3 Contamination Comparison

In general, the contribution of contaminations on different interfaces to the effective dielectric loss is different, even though $\tan\delta_i$, d_{cont} and ϵ_i are the same. Because electric field has different boundary conditions on different interfaces, which gives different participation ratios^[20]:

$$p_{ma}W/d_{ma} = \epsilon_{ma}^{-1} \int ds |E_{a\perp}|^2 \quad (2.3)$$

2. DIELECTRIC LOSS STUDY

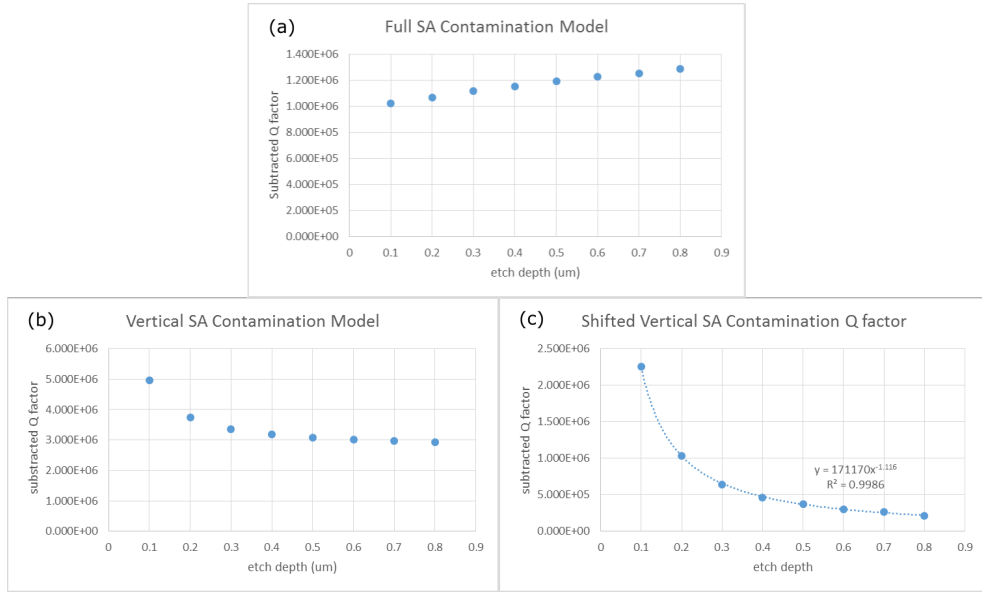


Figure 2.5: Previous Q factors after subtraction of background: (a) result of a model with full substrate-air contamination; (b) result of a model with vertical substrate-air contamination only; (c) result in (b) shifted downward to fit a power function.

Table 2.2: Q factor of model with contamination on different interfaces

Contamination place	ma	sa	ms	every interface
Q factor	4.93×10^6	2.97×10^4	3.45×10^4	2.52×10^5

$$p_{ms}W/d_{ms} = (\epsilon_s^2/\epsilon_{ms}) \int ds |E_{s\perp}|^2 \quad (2.4)$$

$$p_{sa}W/d_{sa} = \epsilon_{sa} \int ds |E_{a\parallel}|^2 + \epsilon_{sa}^{-1} \int ds |E_{a\perp}|^2 \quad (2.5)$$

When $\tan\delta_i$, d_{cont} and ϵ_i are taken to be the same, which is the case in the simulation, p_{ms} and $p_{sa\parallel}$ are two orders of magnitudes larger than p_{ma} and $p_{sa\perp}$. Consequently, dielectric loss on metal-air interface is much smaller than those on metal-substrate and substrate-air interfaces, which focus our attention on the later ones to reduce dielectric loss.

The purpose of this subsection is to verify the validity of above statement. To do this, a model with the potential to put contaminations on every interface is built.

Table 2.2 shows the simulation result of varying contamination position. The relative value among ma, sa and ms is consistent with the theoretical prediction above, i.e. the Q factor of ma contamination is 2 orders of magnitude larger than the other two. However, table 2.2 also shows some inconsistency

(see section 2.3 for detail). Because of the inconsistency and unrealistic resonance frequency, we decided to switch simulation software to SONNET to check the validity of the COMSOL results.

2.2 GHz Resonators

The simulators used in this section are SONNET and Microwave Office.

SONNET is a simulation software designed for high frequency electromagnetic tasks. Unlike COMSOL, in which 3D modeling is possible, SONNET is a 2D modeling tool, in which all metal structures are of no thickness, although multi-layer pseudo-3D modeling is allowed. Even so, some true 3D structures like via and dielectric bricks are allowed in dielectric layers. In SONNET userguide, via (metallic) and dielectric bricks (dielectric) are introduced in detail. In simulation, dielectric bricks can be used to simulate materials in CPW gaps, like air and contamination on the substrate-air interface. However, it is hard to simulate contaminations on vertical interfaces, because the calculation power consumed by dielectric bricks increases dramatically as the area of dielectric material and Z partition (a parameter determining the number of mesh layers in a dielectric layer) increase; furthermore, it is essentially impossible for SONNET to resolve some thin structures like vertical contamination, while keeping the calculation power consumption in a reasonable range.

There is a built-in Q factor calculator in SONNET, however, the result does not seem to make sense in at least our simulation. So equation 1.4 is applied to calculate intrinsic Q factor of the resonator from S parameters.

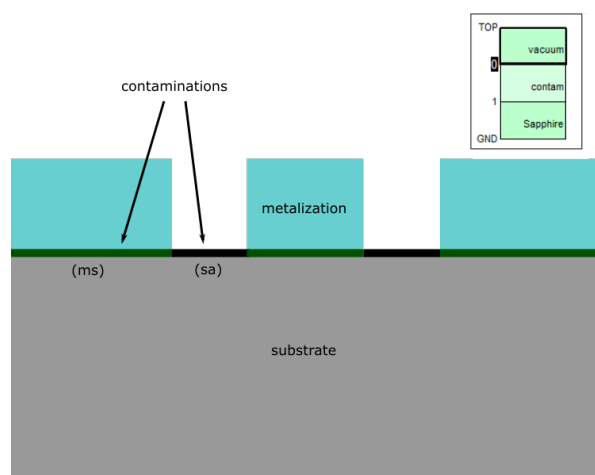


Figure 2.6: First SONNET model: without etch gap and with metal-substrate and substrate-air interfaces contaminations only. The small box on the upright corner is the cross-section shown in SONNET's stackup manager.

Table 2.3: SONNET parameter list

parameters	symbols	standard value
resonator length	L	1.3 (cm)
central line width	S	10 (μm)
coupling capacitor gap width	W	5 (μm)
CPW gap width	W_g	5 (μm)
contamination thickness	d_{cont}	2 (nm)

In all the GHz resonator models in SONNET, the vacuum block above and the substrate are of thickness 500 μm , and the standard values of parameters are listed in table 2.3. Etch depth is not listed here. Because models in subsection 2.2.1 have zero etch depth, while models in other subsections have finite etch depth.

2.2.1 Parametric Sweep

In the model in this subsection, a full CPW resonator is simulated. The cross section of this model can be found in figure 2.6, where only ms and sa contaminations are simulated, and loss tangents of both of the contaminations are set to be 0.002.

The simulation results shown in figure 2.7 is consistent with the result in section 2.1, where COMSOL is used as primary simulation software. Here, the exponent of contamination thickness sweep is -0.986, which is slightly closer to -1 than that of COMSOL simulation. This difference, however, is within the tolerable range of error. Sweeping of other parameters shows no clear correlation with Q factor within the sweeping range, which consists with COMSOL results. The consistency confirms the validity of adopting results from THz regime simulation in COMSOL to GHz regime case.

Because of the limitation of calculation power, contamination comparison will be discussed in subsection 2.2.3 with the help of Microwave office, just as the case of etch depth.

2.2.2 Etch Depth Study

Microwave Office is an easy-to-use simulation software designed for circuit analysis. Though it is hard to design an element from structural level directly in Microwave Office, touchstone files created by SONNET can be imported as subcircuits. In the specific task of CPW resonator, the resonators are divided into several transmission line segments and two coupling capacitors, so that calculation power consumption of analyzing a single element by SONNET is kept in a reasonable range. The subcircuits are then assembled to a resonator in Microwave Office as shown in figure 2.8, and the resulted S parameters show clear signature of resonance, as shown in figure 2.9.

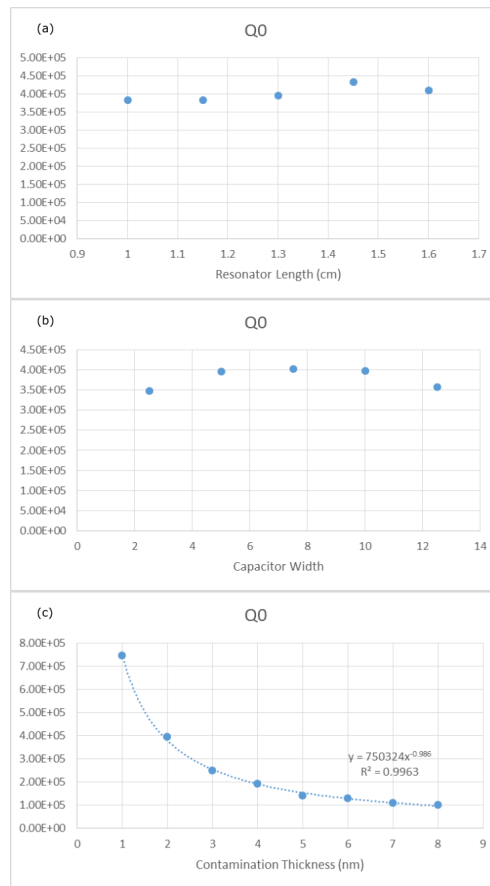


Figure 2.7: Q factor of simulation in SONNET with 0 etch depth: (a) sweep over L ; (b) sweep over W ; (c) sweep over d_{cont} .

However, when the loss tangents of the contaminations are the same as the models in COMSOL and SONNET, this subcircuit method gives a Q factor much higher than the previous cases. To compensate the effect, a much larger loss tangent (0.1) is applied.

Figure 2.10 shows the cross section of the full contamination model in SONNET. In the CPW gaps are dielectric bricks. They embedded in dielectric layers. Dielectric bricks are drawn on the corresponding dielectric layer and extend to the lower bound of the layer above (e.g. contamination bricks are drawn on layer 4, and extend to the lower bound of layer 3). Metalization is drawn on layer 1 (so, on layer 1, there are both metalization and air dielectric bricks).

Figure 2.11 shows the simulation results of horizontal sa contamination models with respect to etch depth. A clear positive correlation of intrinsic Q factor and etch depth is observed. The reason for the increasing is intuitive:

2. DIELECTRIC LOSS STUDY

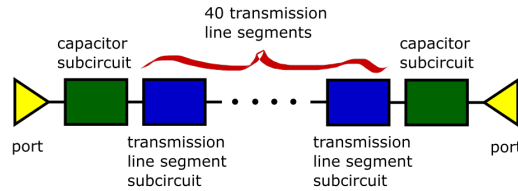


Figure 2.8: The assembled resonator in Microwave Office consists of subcircuits of touchstone files generated by SONNET.

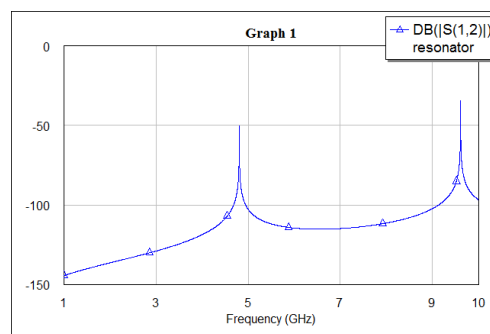


Figure 2.9: S_{12} of an assembled resonator in Microwave Office. Clearly, the method captures the resonance of the structure.

electric field decays fast away from the plane of metalization, and dielectric loss is proportional to $|E|^2$. In figure 2.11 (a), the increasing of intrinsic Q factor reflects the inverse of the decay of $|E|^2$ as indicated by equation 2.2 and equation 1.5. The result points out that by deep etching, the dielectric loss contribution from substrate-air contamination on the bottom of CPW gap can be significantly reduced.

Not only intrinsic Q factors, impedance of the CPW and fundamental resonance frequency also change with etch depth. As shown in figure 2.11 (c) and (e), impedance and resonance frequency follow nearly perfect exponential saturation laws. This study shows a comprehensive effect of deep etching. Deep etching not only reduces dielectric loss, also changes impedance and resonance frequency, which should be paid attention to when fabricating CPW resonators using deep etching method.

Figure 2.12 shows the intrinsic Q factor of a model with metal-substrate contaminations only. No dependence on etch depth is observed. To have a better comparison to the result of COMSOL (remember COMSOL shows a positive correlation in the range from 0 to 80 nm), figure 2.12 (b) studies the behavior in the same range, and again found no dependence. The reason for the inconsistency will be discussed in the subsection 2.2.3.

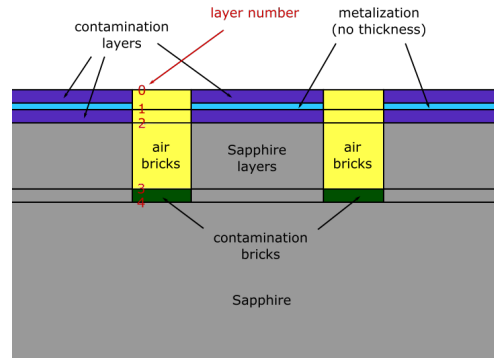


Figure 2.10: Cross section of full contamination model in SONNET with corresponding positions of metalization and dielectric bricks. In the figure, "layer" stands for circuit layers, and "bricks" stands for dielectric bricks.

Table 2.4: Q factor of model with contamination on different interfaces

Contamination place	ma	sa	ms	every interface
Q factor	2.17×10^4	4.61×10^4	9.00×10^3	5.63×10^4

2.2.3 Contamination Comparison

Table 2.4 shows the simulation results of models with contaminations on different interfaces. The etch depths are chosen to be 10 nm for all models. This result is totally different from the result in COMSOL and the theoretical prediction at the beginning of this chapter: here, the relative relation between sa Q factor and ms Q factor is reversed compared to COMSOL result. Furthermore, Q factor of metal-air interface contamination is comparable with the other two (in fact, ma Q factor is even lower than sa Q factor), which contradicts both COMSOL simulation and theoretical prediction.

A possible reason for this inconsistency is the zero-thickness metalization in SONNET, which may leak more electric field into the surrounding lossy materials. Consequently, contaminations right next to metalization (metal-air and metal-substrate) become more lossy than the case in COMSOL (both Q factors reduce significantly relative to that of substrate-air contamination). On the contrary, substrate-air contamination is away from metalization, which gives a more faithful result. So the study on sa contamination and etch depth is still plausible.

2.3 Discussion

From the results listed above, all methods have their advantages and disadvantages, and none of them can simulate a full contamination model plau-

2. DIELECTRIC LOSS STUDY

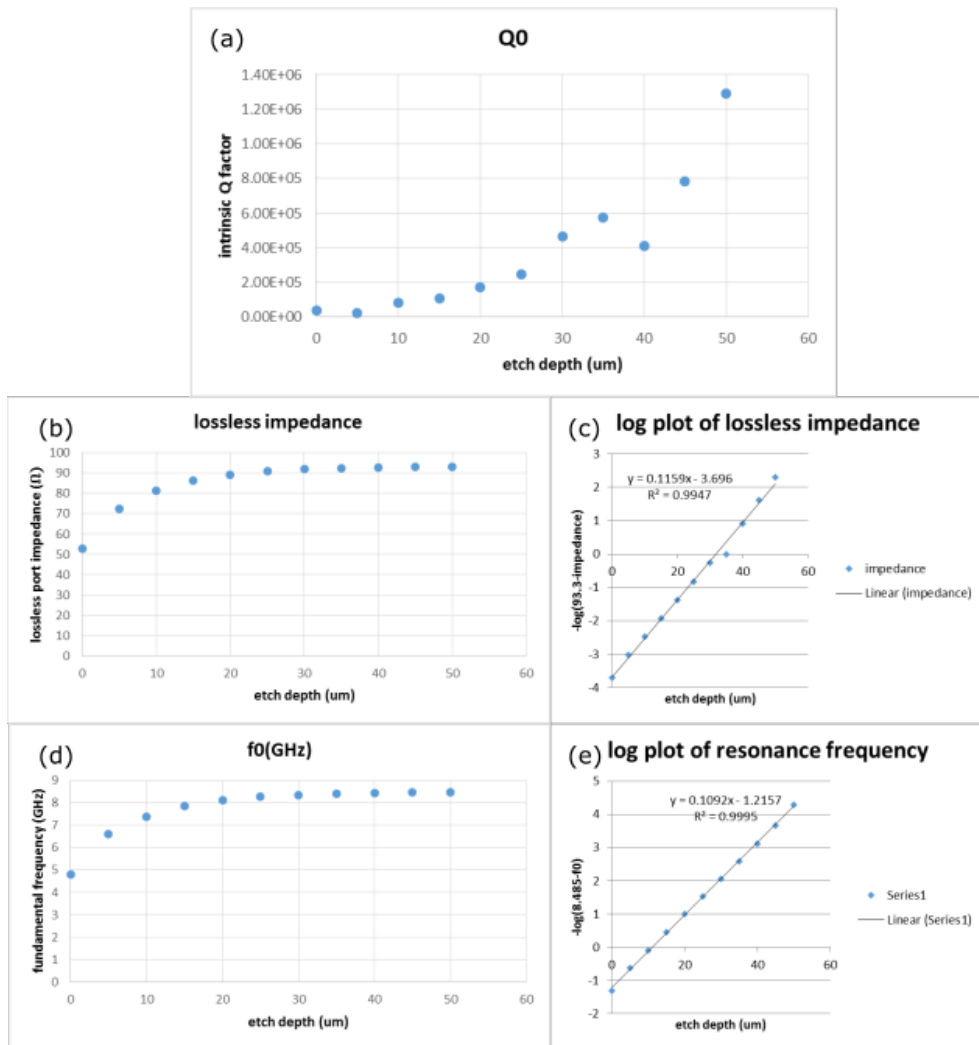


Figure 2.11: Etch depth study of a model with substrate-air contaminations on the bottom of CPW gap only. (a) The intrinsic Q factor shows a clear increase as etch depth increases. (b)(c) Impedance of the CPW resonator shows an exponential saturation as etch depth increases. (d)(e) Fundamental resonance frequency also displays an exponential saturation.

sibly. However, combining the results of the simulations, one can have a comprehensive picture of the dielectric loss in CPW resonator.

2.3.1 Modeling with COMSOL

In the THz resonators section, only metal-substrate and substrate-air contamination models are studied. Because of some bug like problems of COMSOL, it is extremely tedious to sweep parameters in full contamination model. Furthermore, as shown in subsection 2.1.3, the model with full contamination gives a higher Q factor than those with ms and sa contaminations only. This

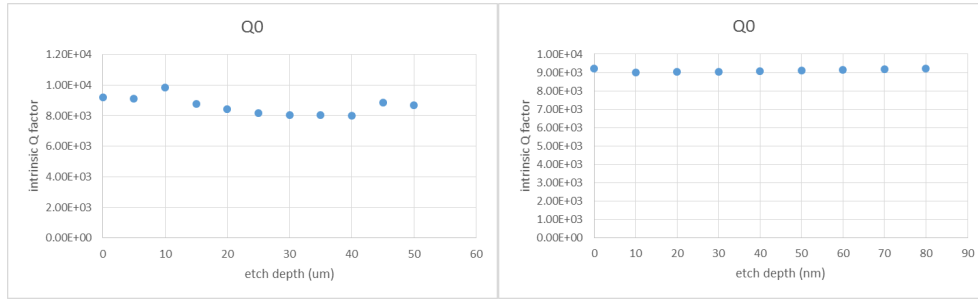


Figure 2.12: Etch depth study of a model with metal-substrate contaminations only. (a) d_{etch} swept from 0 to 50 μm ; (b) d_{etch} swept from 0 to 80 nm. The intrinsic Q factor does not show any dependence on etch depth in either studies.

result does not make sense, because the only differences between the models are materials at the thin layers of contaminations. The 2-nm thick contamination layer should not make much difference in impedance or other parameter, which may influence the Q factor of the model. This result casts doubt on the validity of full contamination model in COMSOL, and persuades us not to conduct parametric sweep in this model.

2.3.2 Etch Depth and Dielectric Loss

In subsection 2.2.2, a clear positive correlation is observed between d_{etch} and Q_0 in a model with horizontal substrate-air contamination only. However, some fluctuations prevent us from determining the exact function of dependence. Power law and exponential law are two straightforward candidates. The clear exponential saturation in etch depth dependences of lossless impedance and resonance frequency infers that the effect of etching on electric field decays exponentially as etch depth increases, which makes the exponential dependence of Q_0 on d_{etch} more favorable. However, in subsection 2.1.2, the power law with exponent close to -1 in vertical sa contamination model infers that participation ratio in unit length along etch depth follows a power law with exponent around -2, because the total dielectric loss is obtained by integrating unit length participation ratio along the etch depth. Subsequently, electric field decays along etched depth following a power law with exponent around -1, as participation ratio is proportional to square of amplitude of electric field (equation 2.5), which suggests another possibility of d_{etch} dependence of electric field.

Though there are some inconsistency, one can safely draw the conclusion that etching into substrate increases the Q factor of a CPW resonator. Because simulation results show clear negative correlation between dielectric loss in SA interface contaminations and etch depth, while show no correlation between dielectric loss in MS interface contaminations and etch depth (SONNET result).

2.4 Conclusion and Outlook

Dielectric loss in a CPW resonator depends on its geometry. Q factor decreases as contamination thickness increases, following a power law with exponent around -1. Q factor of models with contamination on substrate-air interface also has a clear positive correlation with finite depth etching into the substrate below CPW gap. Q factor of models with metal-substrate contamination displays no dependence on etch depth in SONNET and a doubtful positive correlation in COMSOL. Overall, etching into substrate in CPW gap increases Q factor of the models. The simulation results indicate that careful surface treatment of substrate after photolithography (to reduce contaminations) and deep etching can significantly reduce dielectric loss in a CPW resonator. The success of fabricating CPW resonators with Q factor exceeding 1,000,000 using these two methods has been reported during the time of this semester project^[23], which is pretty impressive.

Future work can be done on the origin of dielectric loss as inspired by [21]. By controlling the exposure to water and acid material during fabrication, one may be able to study the contribution of Hydrogen bonds to dielectric loss.

Appendix A

COMSOL RF Module Manual

COMSOL is a powerful and widely used simulation tool for various of physical tasks. However, to my knowledge, there is no good manual or tutorial available on the Internet. Most of my knowledge comes from the built-in dynamic help (the button can be found at the top-right corner of corresponding settings window (the window in the middle of the three) as a shape of computer with a question mark) and by studying similar models in model library (can be found in Dynamic Help → Contents → Model Library). This appendix will introduce some basic functions and tricks of COMSOL RF Module.

A.1 Build A New Model

When a new project is created, model wizard will automatically appear as the settings window on the interface. One can choose the dimension, physics and study type of the model one after another, following the guidance of the wizard and click "next" arrow on the top-right corner of model wizard to confirm the choice. After finishing all the choices, click the "finish flag" on the top-right corner to finalize the selections. It is possible to add/remove physics and study types at any time in the model builder window (the left most window on the interface) by right clicking the corresponding node.

A.2 Global Parameters

Using self-defined parameters, instead of using numbers everywhere, sometimes can save a lot of work during the simulation, especially when something needs to be changed.

One can define a list of global parameters by right clicking "Global Definitions" node in model builder window (the leftmost window on the interface), and selecting parameters. The expressions of parameters can either be

a number or a mathematical expression with built-in or self-defined parameters. The scopes of the parameters are global, so that they can be called anywhere in the project.

A.3 Port and Lumped Port

Under the "Electromagnetic Waves, Frequency Domain" (a kind of physical situation available in COMSOL) node in Model Builder window, one can specify boundary conditions. Boundary conditions are crucial in a electromagnetic wave problem. Wrong choice of boundary conditions may lead to highly unphysical results. Some of the boundary conditions introduced here are also available in some other physics related to electromagnetic field.

The default boundary condition on the surface of the model is "Perfect Electric Conductor" (a small "D" on its node indicating it is default), the detailed properties can be found in dynamic help. This boundary condition can be overwritten by other self-chosen ones. Different from self-chosen perfect electric field, the default one cannot be defined on any interior boundaries of the model.

For a circuit-like model, the most important boundary conditions are port and lumped port, where electromagnetic energy enters or exits the model (for eigenfrequency study, port or lumped port is not necessary).

A port is supposed to be surrounded by metallic boundaries, e.g. perfect electric conductor or other metals. On the top of settings window of port is boundary selection tap. One can select the desired boundaries by left click followed by right click in Graphic window. Under Port Properties tap, port name, port type, excitation, input power, port phase can be specified. Port type should be adjusted according to the geometry of the port: rectangular for rectangular port, coaxial for coaxial ones, user defined for other shape. For user defined port type, input electromagnetic field should be specified in Port Mode Settings tap; for rectangular port, mode type (TE, TM and so on) should be specified.

A lumped port is supposed to be located between two metallic boundaries (if it is surrounded by metallic boundaries, COMSOL will return an error at run time). A lumped port is a justified approximation to port, when the distance between two metallic boundaries is much smaller than wavelength. Coaxial, uniform and user defined port types are available for lumped port. User defined port type is basically similar to uniform one (both of them deal with uniform field), but with more freedom in boundary shape and range. Instead of specifying input electromagnetic wave, lumped port requires specifying characteristic impedance.

A.4 Mesh

Computers cannot solve truly continuous problem, so mesh is required to reduce continuous problems to discrete problems. The finer the mesh is, the more accurate the solution is. However, calculation power and calculation time consumption increases linearly with total number of mesh elements.

For normal tasks, the automatic free tetrahedral mesh is enough. When some structure requires finer mesh, the corresponding mesh can be built manually by right clicking mesh node and selecting a specific mesh type, selecting the desired objects in Graphics window (the rightmost window), and specify the size of mesh by right clicking the corresponding mesh option node and add a size controller.

For thin layers, usually COMSOL could not manage building mesh inside these structures. Because the difference between edges of automatic mesh element cannot be too big, which results in too many mesh elements in thin layers. To resolve the problem, one can build surface mesh using options like free triangular on one broad boundary of the thin layer, and sweep the surface mesh to the other broad boundary by adding a "sweep" by right clicking mesh node. In principle, many thin-layer structures can be replaced by transition boundary condition, but we did not manage to do that.

A.5 Eigenfrequency Study

Eigenfrequency study is used when the properties of eigenmodes are interested. Resonance mode of a resonator is a good example.

Under the node of eigenfrequency study, there is a default solver property node called "Step 1: Eigenfrequency". Selecting it, and the corresponding settings window appears. Under the "Study Settings" tap, two parameters "desired number of eigenfrequencies" and "search for eigenfrequencies around" should be specified. If the specified frequency is far from any eigenfrequency of the model, COMSOL would not be able to find resonant modes and will keep running, till some non-resonant solution comes about or finish the desired number of iterations (this can be set by right clicking eigenfrequency study node → Show Default Solver → corresponding solver → corresponding eigenvalue solver → Advanced tap → Maximum number of eigenvalue iterations), so an estimation of desired eigenfrequency is important when using eigenfrequency study. One can also change the accuracy of the solution by right clicking eigenfrequency study node finding "Show Default Solver" → corresponding solver → corresponding eigenvalue solver → General → Relative tolerance. In general, the lower the relative tolerance is, the higher the accuracy is, but the longer it takes to solve the problem.

Please notice that if relative tolerance is too low, highly inaccurate solution may appear.

One can also define parametric sweep in the solver to combine several studies in one by right clicking study node, selecting parametric sweep. Please notice that parametric sweep on the model geometry is only valid to a geometry built in COMSOL. Under "Study settings" tap, one can add parameters to be swept by clicking the "+" button, and choose the desired one from the pull-down menu. In principle, multi-parametric sweep is possible, and will return a matrix (tensor for higher dimensional case) of solutions. However, in practice, this can be problematic.

After finishing all the study settings, one can simulate the model by right clicking the study node, selecting "Compute". The progress can be monitored by selecting the "Progress" tap in the bottom-right window. The memory consumption is also shown at the bottom-right corner of the interface. If the model is too complicated, COMSOL may use up all the memory and cause some problems.

When the computation finishes, the default setting result will be displayed automatically in Graphics window. One can change the displayed result by selecting solution from Settings window → Data tap → Data → Data set and Eigenfrequency. Other plot settings like color legend can also be changed in this window. By selecting the "Multislice" node under the corresponding solution node, the position and number of slice can be specified. More importantly, the plotted expression can be selected by clicking the double arrow button at the top-right corner of "Expression" tap in settings window. Electromagnetic field related quantities can be found in "Electromagnetic Waves, Frequency Domain". Most frequently used Q factor can be found in "Electromagnetic Waves, Frequency Domain" → Global → Quality factor.

Eigenfrequency study cannot be used to determine S parameters (ports are not necessary in this study type after all). To get S parameters, one should conduct frequency domain study, which is not introduced here.

A.5.1 Graphics Window

Graphic window is the rightmost window on COMSOL interface, and is the place where the geometry of the model and plot of results are displayed. It is convenient to know some tricks of using graphic window.

One can rotate the graph in 3D by dragging it with left mouse button, and move it parallelly by dragging with right mouse button.

Figure A.1 shows a screen shot of graphic window. There are a row of functional buttons to control the display of the graph. The buttons are grouped

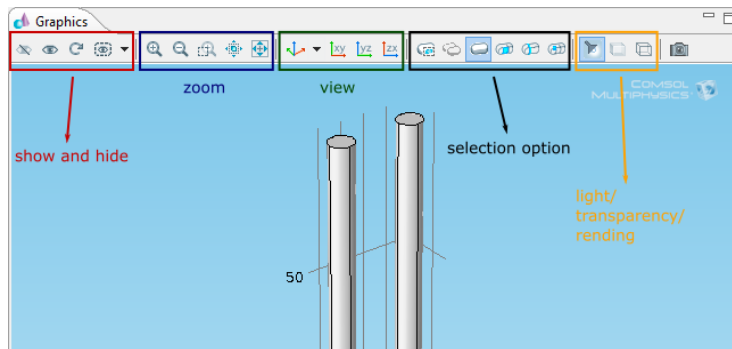


Figure A.1: Screen shot of graphics window in COMSOL.

as functional groups: show and hide, zoom, view, selection option and some other functions from left to right.

Show and hide functions are useful when the model is complicated and some parts are blocked by others. In this case, one can hide the objects blocking the objects in interest, and work on those interested ones directly. Hidden objects cannot be selected directly in graphic window, which is crucial for selecting blocked object in complicated model. (If the structure is not too complicated, one can select a blocked object by selecting the front-most object, and clicking at the same place again.) To my knowledge, hidden objects can only be reset to "shown" by "Reset Hiding" function (which set all objects as "shown") or select them in settings window under nodes like Materials and press "Show Selected".

View functional group provides four standard views for users to go to whenever they are needed. The function is useful as it is hard to control the rotation of model in graphics window.

In the rightmost functional group are "Scene Light", "Transparency" and "Wireframe Rendering" buttons. "Scene Light" function turns on and off a light shining on the model. When light is on, the model looks more "3D", but may sometimes make it hard to see the structure. "Transparency" function turns on and off the transparent mode. However, left clicking still primarily selects the front-most object in transparent mode. "Wireframe Rendering" function can change the view of a model into framework only mode. Similar to transparent mode, wireframe rendering mode does not change the priority of selection.

Appendix B

SONNET Manual

New user of SONNET can follow the guidance in Quick Start Guide window to create basic model and conduct analysis. If Quick Start Guide window does not appear automatically, it can be found under Help → Quick Start Guide. A well-written SONNET user's guide can be found online, with introduction to most functions and tasks^[27]. In this manual, I will focus on dielectric bricks, an advanced and hard-to-control function. More details can be found in SONNET user's guide.

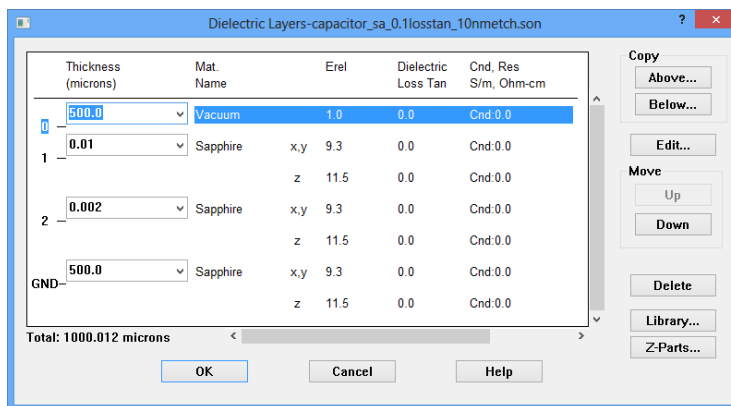


Figure B.1: Dielectric layer editor window in SONNET.

Before we introduce dielectric bricks, I would like to introduce some basic concepts about dielectric layers first. Figure B.1 shows the dielectric layer editor window. One can specify the properties like thickness, material, Z partition of each dielectric layer, copy and move layers. The most important thing to pay attention to is the way SONNET numbers the layers. Layers are numbered by the lower bound, and counted from top to bottom, starting from 0 and ending with GND (ground). Ground is the bottom of the model,

and 0 layer extend to the top of the model. Metals are drawn on the interfaces of dielectric layers, sharing the same number as the dielectric layer above, and are primarily thin (without thickness). With these concepts in mind, dielectric bricks can be introduced more clearly.

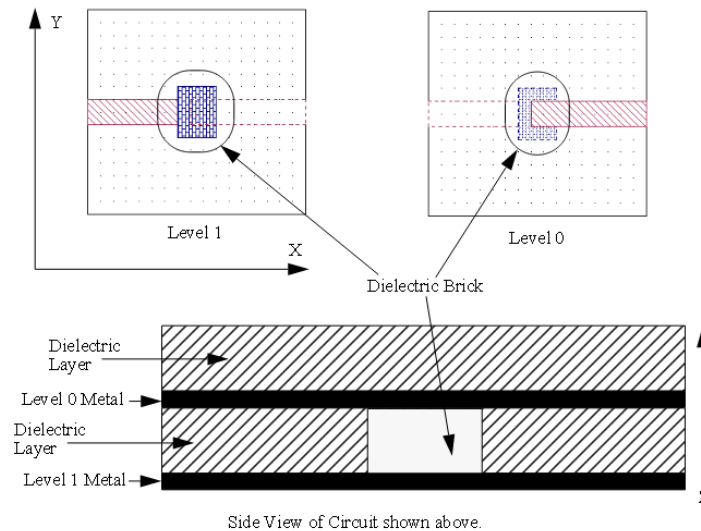


Figure B.2: [27] Views of dielectric bricks

A dielectric brick is a solid volume of dielectric material embedded within a dielectric layer. A partially Z-direction-extended dielectric brick in a layer is not possible, which can only be achieved by adding dielectric layers. Figure B.2 shows the top view on the level where the base of dielectric brick is located, the top view on the level above and the side view (not available in SONNET) respectively of a circuit containing a dielectric brick. On the base level, the brick is shown in solid line; while on the level above, it is shown in dashed line. Dielectric bricks should be created on the level where its base is located.

Whenever there are dielectric bricks in a dielectric layer, the Z partition should be specified for the layer. The default Z partition is 0, which will make SONNET return an error at run time. The more Z partition is in a layer, the more accurate the result is. However, calculation power consumption increases dramatically as the area of the dielectric brick and Z partition of the corresponding dielectric layer increase. So dielectric bricks should only be used very locally. When the thickness of the dielectric layer changes, Z partition should be changed too. Figure B.3 shows the consequence of keeping Z partition the same while changing etch depth: the model hits some unphysical resonance. To my knowledge, it is best to keep the ratio between Z partition and dielectric layer thickness the same, whenever it is

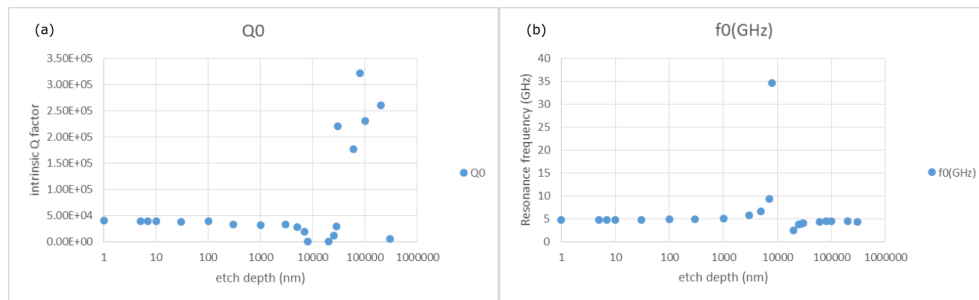


Figure B.3: Etch depth study with the same Z partition of etch gap layer. The model "hits some unphysical resonance" at etch depth around 10 μm , with intrinsic Q factor goes to 0 and resonance frequency goes to infinity. At some points, no resonance can be observed in Microwave Office.

possible. Etch depth study with sa contamination on the bottom of CPW gap applies the method. When the etch depth is 5 μm , Z partition is 5; when etch depth is 10 μm , Z partition is 10 *etc.*

Appendix C

Xmon Capacitor

Xmon is a recently developed superconducting qubit with long coherence time, straightforward connectivity and fast control^[28]. Before I started working on CPW resonators, I simulated an Xmon capacitor model using Ansoft Maxwell. The result shows that the circuit quantum electrodynamical (circuit QED) properties of an Xmon are pretty close to a transmon qubit.

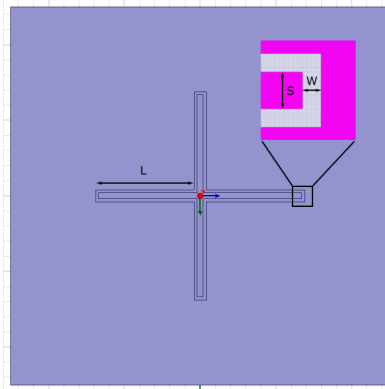


Figure C.1: Top view of Xmon capacitor in Maxwell.

Table C.1: Simulated and experimental values of parameters of Xmon qubits.

S (μm)	8	16	24
W (μm)	4	8	12
L (μm)	130	130	130
Simulated Capacitance (pF)	0.0827	0.0824	0.0829
Simulated E_C (GHz)	0.2342	0.2351	0.2336
Experimental E_C (GHz)	0.206	0.210	0.204
Experimental Anharmonicity (GHz)	0.224	0.228	0.222

C. XMON CAPACITOR

Figure C.1 shows the top view of Xmon capacitor in Maxwell, with geometric parameters indicated in the figure. The materials are Aluminum for metalization, sapphire for substrate, and vacuum for gaps. For simplicity, no qubit or transmission line is coupled to the capacitor.

Table C.1 lists some parameters of simulated and experimental results. Roughly 10% deviations in E_C are observed for all models, and the experimental E_C 's are more sensitive to the change of geometry than simulated ones. Both of the deviations may be explained by the coupling to SQUID and transmission lines in experiment. In transmon qubits, anharmonicity $\alpha \approx -E_C$ ^[18]. The experimental E_C 's agree well with the anharmonicity in [28] except some reasonable deviations, which may be caused by coupling. Both E_C and anharmonicity indicate that Xmon is close to transmon in the sense of circuit QED properties.

Bibliography

- [1] P. W. Shor, "Polynomial-time algorithms for prime factorization and discrete logarithms on a quantum computer," *arXiv: quant-ph/9508027v2*, 1996.
- [2] L. K. Grover, "A fast quantum mechanical algorithm for database search," *arXiv: quant-ph/9605043*, 1996.
- [3] C. H. Bennett and G. Brassard, "Quantum cryptography: Public key distribution and coin tossing," *IEEE Systems and Signal Processing*, volume 175, page 8. New York, 1984.
- [4] D. DiVincenzo, "Topics in quantum computers," *arXiv:cond-mat/9612126*, 1996.
- [5] A. Wallraff, "Qsit notes," 2014.
- [6] A. Blais, R. S. Huang, A. Wallraff, S. M. Girvin, and R. J. Schoelkopf, "Cavity quantum electrodynamics for superconducting electrical circuits: An architecture for quantum computation," *Phys. Rev. A* 69, 062320, 2004.
- [7] D. I. Schuster, A. Wallraff, A. Blais, L. Frunzio, R.-S. Huang, J. Majer, S. M. Girvin, and R. J. Schoelkopf, "Erratum: ac stark shift and dephasing of a superconducting qubit strongly coupled to a cavity field," *Phys. Rev. Lett.* 94, 123602, 2005.
- [8] J. Majer, J. M. Chow, J. M. Gambetta, B. R. J. Jens Koch, J. A. Schreier, L. Frunzio, D. I. Schuster, A. A. Houck, A. Wallraff, A. Blais, M. H. Devoret, S. M. Girvin, and R. J. Schoelkopf, "Coupling superconducting qubits via a cavity bus," *Nature* 449, 443-447, 2007.

- [9] E. Lucero, M. Hofheinz, M. Ansmann, R. C. Bialczak, N. Katz, M. Neeley, A. D. O'Connell, H. Wang, A. N. Cleland, and J. M. Martinis, "High-fidelity gates in a single josephson qubit," *Phys. Rev. Lett.* *100*, 247001, 2008.
- [10] L. DiCarlo, J. M. Chow, J. M. Gambetta, L. S. Bishop, B. R. Johnson, D. I. Schuster, J. Majer, A. Blais, L. Frunzio, S. M. Girvin, and R. J. Schoelkopf, "Demonstration of two-qubit algorithms with a superconducting quantum processor," *Nature* *460*, 240-244, 2009.
- [11] P. K. Day, H. G. LeDuc, B. A. Mazin, A. Vayonakis, and J. Zmuidzinas, "A broadband superconducting detector suitable for use in large arrays," *Nature* *425*, 817-821, 2003.
- [12] A. Endo, C. Sfiligoj, S. J. C. Yates, J. J. A. Baselmans, D. J. Thoen, S. M. H. Javadzadeh, P. P. van der Werf, A. M. Baryshev, and T. M. Klapwijk, "," *Appl. Phys. Lett.* *103*, 032601, 2013.
- [13] M. Göppl, A. Fragner, M. Baur, R. Bianchetti, S. Filipp, J. M. Fink, P. J. Leek, G. Puebla, L. Steffen, and A. Wallraff, "Coplanar waveguide resonators for circuit quantum electrodynamics," *Journal of Applied Physics* *104*, 113904, 2008.
- [14] I. Wolff, *Coplanar Microwave Integrated Circuits*. John Wiley & Sons, 2006.
- [15] C. A. Mack, "Semiconductor lithography (photolithography) - the basic process," 2015.
- [16] S. Gevorgian, P. L. Linner, and E. L. Kollberg, "Cad models for shielded multilayered cpw," *IEEE Transactions on Microwave Theory Techniques*, vol. 43, pp. 772-779, 1995.
- [17] K. Watanabe, K. Yoshida, T. Aoki, and S. Kohjiro, "Kinetic inductance of superconducting coplanar waveguides," *Japanese journal of applied physics*, vol. 33, no. 10R, p. 5708, 1994.
- [18] J. Koch, T. M. Yu, J. Gambetta, A. A. Houck, D. I. Schuster, J. Majer, A. Blais, M. H. Devoret, S. M. Girvin, and R. J. Schoelkopf, "Charge-insensitive qubit design derived from the cooper pair box," *Phys. Rev. A* *76*, 042319, 2007.
- [19] R. Barends, N. Vercrayssen, A. Endo, P. J. de Visser, T. Zijlstra, T. M. Klapwijk, P. Diener, S. J. C. Yates, and J. J. A. Baselmans, "Minimal resonator loss for circuit quantum electrodynamics," *Appl. Phys. Lett.* *97*, 023508, 2010.

-
- [20] J. Wenner, R. Barends, R. C. Bialczak, Y. Chen, J. Kelly, E. Lucero, M. Mariantoni, A. Megrant, P. J. J. O'Malley, D. Sank, A. Vainsencher, H. Wang, T. C. White, Y. Yin, J. Zhao, A. N. Cleland, and J. M. Martinis, "Surface loss simulations of superconducting coplanar waveguide resonators," *Applied Phys. Lett.* 99, 113513, 2011.
- [21] L. Gordon, H. Abu-Farsakh, A. Janotti, and C. G. V. de Walle, "Hydrogen bonds in Al_2O_3 as dissipative two-level systems in superconducting qubits," *Scientific Reports* 4, 7590, 2014.
- [22] W. A. Phillips, "Tunneling states in amorphous solids," *Journal of Low Temperature Physics*, Vol 7, No. 3/4, 1972.
- [23] A. Bruno, G. de Lange, S. Asaad, K. L. van der Enden, N. K. Langford, and L. DiCarlo, "Reducing intrinsic loss in superconducting resonators by surface treatment and deep etching of silicon substrates," *arXiv:1502.04082v1*, 2015.
- [24] D. M. Pozar, *Microwave Engineering*. John Wiley & Sons, 2012.
- [25] N/A, "Maxwell's equations," 2014.
- [26] J. Gao, M. Daal, A. Vayonakis, S. Kumar, J. Zmuidzinis, B. Sadoulet, B. A. Mazin, P. K. Day, and H. G. Leduc, "Experimental evidence for a surface distribution of two-level systems in superconducting lithographed microwave resonators," *Applied Physics Letters*, vol. 92, no. 15, pp. 152505–152505, 2008.
- [27] Sonnet, "Sonnet user's guide," 2013.
- [28] R. Barends, J. Kelly, A. Megrant, D. Sank, E. Jeffrey, Y. Chen, Y. Yin, B. Chiaro, J. Mutus, C. Neill, P. O'Malley, P. Roushan, J. Wenner, T. C. White, A. N. Cleland, and J. M. Martinis, "Coherent josephson qubit suitable for scalable quantum integrated circuits," *Phys. Rev. Lett.*, vol. 111, p. 080502, Aug 2013.



Eidgenössische Technische Hochschule Zürich
Swiss Federal Institute of Technology Zurich

Declaration of originality

The signed declaration of originality is a component of every semester paper, Bachelor's thesis, Master's thesis and any other degree paper undertaken during the course of studies, including the respective electronic versions.

Lecturers may also require a declaration of originality for other written papers compiled for their courses.

I hereby confirm that I am the sole author of the written work here enclosed and that I have compiled it in my own words. Parts excepted are corrections of form and content by the supervisor.

Title of work (in block letters):

Dielectric Loss Study in Superconducting Coplanar Waveguide Resonators
--

Authored by (in block letters):

For papers written by groups the names of all authors are required.

Name(s):

Chen

First name(s):

Junxin

With my signature I confirm that

- I have committed none of the forms of plagiarism described in the '[Citation etiquette](#)' information sheet.
- I have documented all methods, data and processes truthfully.
- I have not manipulated any data.
- I have mentioned all persons who were significant facilitators of the work.

I am aware that the work may be screened electronically for plagiarism.

Place, date

Zurich, 2015/09/02

Signature(s)

Chen Junxin

For papers written by groups the names of all authors are required. Their signatures collectively guarantee the entire content of the written paper.